



# Estimating $\chi_{\text{top}}$ lattice artifacts from flowed SU(2) calorons

P. Thomas Jahn<sup>1</sup>, Guy. D. Moore<sup>1</sup>, Daniel Robaina<sup>1,2,a</sup>

<sup>1</sup> Institut für Kernphysik (Theoriezentrum), Technische Universität Darmstadt, Schlossgartenstraße 2, 64289 Darmstadt, Germany

<sup>2</sup> Max-Planck-Institut für Quantenoptik, Hans-Kopfermann-Straße 1, 85748 Garching, Germany

Received: 14 January 2019 / Accepted: 1 June 2019 / Published online: 15 June 2019

© The Author(s) 2019

**Abstract** Lattice computations of the high-temperature topological susceptibility of QCD receive lattice-spacing corrections and suffer from systematics arising from the type and depth of gradient flow. We study the lattice spacing corrections to  $\chi_{\text{top}}$  semi-analytically by exploring the behavior of discretized Harrington–Shepard calorons under the action of different forms of gradient flow. From our study we conclude that  $N_\tau = 6$  is definitely too small of a time extent to study the theory at temperatures of order  $4 T_c$  and we explore how the amount of gradient flow influences the continuum extrapolation.

## 1 Introduction

Quantum chromodynamics fields generically contain topological structure, which may play a role in some low-energy phenomenology and have been treated extensively in the literature [1]. This paper shall put the focus on topology at high temperatures  $T \gg T_c$  the (crossover) temperature. At these temperatures, the topological susceptibility – the mean-squared  $Q$ -value per unit 4-volume – is small, but it nevertheless plays a crucial role in the cosmological physics of the QCD axion [2–7], should it exist. In this case, besides the now rather well-determined value of the topological susceptibility in vacuum [8], we also need the topological susceptibility in the temperature range  $3 T_c - 7 T_c$  [9, 10], since this is the temperature range where a cosmological axion density would be established. The exploration of topological susceptibility at high temperatures within QCD has recently become the topic of intense investigation [11–18]. (For a recent review of the axion see Ref. [19].)

At low temperatures, topology is dominated by long range physics where the coupling is strong. In this regime, we have little rigorous theoretical guidance for the form of the configurations which predominantly contribute to the topologi-

cal susceptibility. On the other hand, at high temperatures the coupling is weak and Gross, Pisarski, and Yaffe [20] demonstrated that the dominant configurations are expected to be calorons (periodic instantons) with radius  $\rho$  of order of half the inverse temperature. Smaller objects are suppressed by the smaller coupling at short distances, and larger objects are suppressed by their interaction with thermal fluctuations. In general, at high temperatures, topological objects are rare and can be treated singly (dilute instanton gas).

At the temperature range relevant for axion cosmology, topological objects should be dilute, but corrections to perturbation theory may be large. In particular, the calculation of the thermal corrections to the caloron action is not secure due to the infrared issues of thermal fluctuations which exist even at weak coupling in gauge theories [8, 21]. Those can influence the environment of the caloron and change the exact coefficient of the  $\exp(-\rho^2 T^2)$  suppression of large calorons. Therefore a nonperturbative lattice treatment would be very valuable. But this brings with it some complications. Strictly speaking, there is no perfectly clean and unambiguous definition for topology on the lattice. After all, on a compact space without boundary, topology partitions the space of smooth continuum configurations into path-disconnected subspaces with different integer  $Q$  values. But the space of lattice configurations is  $[\text{SU}(N)]^{N_\ell}$  (with  $N_\ell$  the number of lattice links), which is path connected, precluding a continuous and integer definition of  $Q$ . This problem has long been appreciated; Lüscher showed that topology becomes well defined if we restrict to sufficiently “smooth” lattice configurations, in the sense that all plaquettes are suitably close to the identity [22]. That means that the failure for a perfectly clean definition of topology on the lattice lies with certain very non-smooth configurations, termed “dislocations.”<sup>1</sup>

<sup>a</sup> e-mail: [daniel.robaina@mpq.mpg.de](mailto:daniel.robaina@mpq.mpg.de)

<sup>1</sup> Of course topology can be given a rigorous definition, for instance, by the signed sum of zero modes of a Ginsparg–Wilson [23] fermionic

A modern tool for studying topology on the lattice is the integration of a lattice discretized version of  $Q$  after the lattice fields have been subjected to gradient flow [26, 27]. This definition has its roots in older studies employing *cooling* [28–31], with gradient flow representing a better-controlled and better-understood form of gauge-link cooling. With gradient flow, a well-defined parameter  $t$  controls the extent of smearing applied. Gradient flow tends to eliminate dislocations [32], but since there is no clean distinction between dislocations and small-but-physical instantons, it may also destroy the smallest instantons which we want to keep. This issue is addressed phenomenologically in most lattice studies that attempt a calculation of the topological susceptibility, but we are surprised by the absence of a more systematic study, which might help in understanding how wide the flow time window actually is, and how large we should expect the lattice artifacts in the topological susceptibility to be. In other words, it would be useful to get a better analytical understanding of how lattice spacing and flow-depth effects may influence the determined topological susceptibility.

In this paper we shall explore this issue by studying exactly how much gradient flow destroys exactly what size of Harrington–Shepard calorons [33]. This requires a lattice implementation of the caloron, which we supply. We also explore different implementations of gradient flow: (a) Wilson flow [27], (b) a recently proposed  $\mathcal{O}(a^2)$ -improved flow dubbed Zeuthen flow [34], and (c) an “overimproved” flow in which we force the  $a^2$  errors in the flow action to have the opposite sign as in Wilson flow. We are hardly the first to implement discretized topological configurations on the lattice [35–37] or to consider topology after cooling [29–31, 38, 39]. But our emphasis is a little different; we want to understand and control what size of dislocation/caloron survives what amount of flow, and what impact this may have on the determination of the topological susceptibility at finite lattice spacing and on the corresponding extrapolation to the continuum limit.

A natural objection to our study is that, in the temperature range of relevance, the coupling is still quite large. Therefore, the actual topological objects from the lattice will not be clean calorons, but will have large fluctuations. Nonetheless, gradient flow will drive any topological object towards a caloron solution in a much smaller amount of flow time than it takes for the object to disappear, since the caloron is a stationary point of the action up to  $a^2$  corrections. Therefore the actual

topological objects’ flow trajectories should be very similar to those for calorons. (In fact, in the continuum, we could even define the size of a topological object to be the size of the caloron it approaches under gradient flow.) Therefore our study can still shed light on how much flow removes what size of topological object. Combining this with an estimate, based on Gross Pisarski and Yaffe’s work, for the size distribution of calorons, can illuminate what flow depths affect the topological objects we want to keep, and what lattice spacings may be too coarse to distinguish between dislocations and physically relevant topological objects.

The paper is structured as follows: In Sect. 2 we collect our definitions and define our topology configurations at finite temperature. Section 3 then introduces the different flows and flow actions. In Sect. 4 we compute  $\rho_{\text{crit}}(t)$  which indicate the value of the radius of a caloron that barely survived the amount of flow time  $t$ . These curves are further used in Sect. 5 to estimate how lattice spacing systematics interfere with flow effects in the approach to the continuum. An example study at  $T = 4 T_c$  is used. Our conclusions can then be found in Sect. 6.

## 2 Caloron discretization with $Q = 1$

The Harrington–Shepard caloron [33] can be understood as the finite temperature generalization of the BPST instanton [40]. The most straightforward way of constructing the solution is to recognize that one has to take into account the infinite time copies that arise due to the compactification of the Euclidean time direction whose inverse length plays the role of temperature ( $\beta \equiv T^{-1}$ ). Following [41] we consider a superpotential of the form

$$\begin{aligned} \Phi_{\text{HS}}(x) &= 1 + \sum_{k \in \mathbb{Z}} \frac{\rho^2}{(x - z_k)^2} \\ &= 1 + \frac{\pi \rho^2 \sinh \frac{2\pi |\mathbf{x} - \mathbf{z}|}{\beta}}{\beta |\mathbf{x} - \mathbf{z}| \left( \cosh \frac{2\pi |\mathbf{x} - \mathbf{z}|}{\beta} - \cos \frac{2\pi (x_0 - z_0)}{\beta} \right)}, \end{aligned} \quad (1)$$

with  $z_k = (z_0 + k\beta, \mathbf{z})$  and  $\rho$  having length-units and playing the role of the caloron radius. Concentrating on  $\text{SU}(2)$  calorons, the gauge field continuum form is obtained via

$$A_\mu^a(x) = \eta_{a\mu\nu} \partial_\nu \ln \Phi_{\text{HS}}(x) \quad (2)$$

where  $\eta_{a\mu\nu} = \epsilon_{0a\mu\nu} + \delta_{a\mu} \delta_{\nu 0} - \delta_{a\nu} \delta_{\mu 0}$  is the ’t Hooft symbol (equivalently for  $\bar{\eta}_{a\mu\nu}$  the sign of the last two terms is reversed and one obtains an anti-instanton with  $Q = -1$ ) [40]. The self-duality condition  $F_{\mu\nu} = \frac{1}{2} \epsilon_{\mu\nu\rho\sigma} F_{\rho\sigma}$ , implies that a valid solution for  $A_\mu(x)$  is obtained if  $\Phi_{\text{HS}}(x)$  obeys the Poisson equation  $\square \Phi_{\text{HS}} = 0$ .

Footnote 1 continued

operator. However this definition is not unique, since there are multiple choices for Ginsparg–Wilson operators. For instance, those operators constructed by the overlap method [24, 25] are dependent on specific choices in the Wilson operator used to build the overlap operator. Roughly speaking, dislocations are those configurations which will give different values of topology for different implementation choices.

It is a tedious but straightforward exercise to check that indeed this gauge field yields  $Q = 1$  and  $S = 8\pi^2$ . Notice that it is given in singular gauge, meaning that there is a singularity at the center of the caloron when  $x = z$ .<sup>2</sup> Next, we use the path-ordered exponential map to obtain the expression for the lattice links as

$$U_\mu(x) = \mathcal{P} \exp \left[ a \int_0^1 dt A_\mu (\Gamma_\mu(x, t)) \right], \tag{3}$$

where  $\Gamma_\mu(x, t) = x + ta\hat{\mu}$  is an appropriate parameterization for the corresponding path connecting the two neighboring lattice sites  $x$  and  $x + a\hat{\mu}$  with  $t \in [0, 1]$  (no summation over  $\mu$  is implied in Eq. (3)).

In the case of an instanton (without periodic images),  $A_\mu$  commutes everywhere along a link, but this turns out not to be true for the caloron. In order to compute the links we rewrite Eq. (3) as a product of  $n$  shorter links,

$$U_\mu(x) = \lim_{n \rightarrow \infty} \mathcal{P} \prod_{k=1}^n \exp \left[ \frac{a}{n} A_\mu \left( \Gamma_\mu \left( x, \frac{2k-1}{2n} \right) \right) \right], \tag{4}$$

where in practice we use  $n \sim 40$  rather than taking the strict  $n \rightarrow \infty$  limit. Periodicity is imposed in all four dimensions, and while boundary effects are absent in the time direction, our lattice field will have a discontinuity at the spatial edges of the box. We ameliorate this problem with gradient flow confined to the boundary region as described in App. A.

Finally the embedding into an SU(3) background is trivial since a particular lattice gauge exists in which the links take the following form:

$$U_\mu^{\text{SU}(3)} = \begin{pmatrix} U_\mu^{\text{SU}(2)} & 0 \\ 0 & 1 \end{pmatrix}. \tag{5}$$

Therefore we are *effectively* considering SU(2) configurations in this paper. This makes our study less general than Ref. [36], who also consider calorons in the background of nontrivial holonomy. Note, however, that if we are primarily interested in *high* temperatures, nontrivial holonomy is not likely to be relevant, since fluctuations create an effective potential for the Polyakov loop which favors trivial holonomy [20].

### 3 Gradient flows

Gradient flow and its discretized version on the lattice [26,27,42–45] have become an essential tool to reduce UV fluctuations. In the continuum it defines a mapping of the

<sup>2</sup> On the lattice, we will avoid the singularity by placing our topology objects in between lattice points and unless stated otherwise we always consider  $z = (z_0, \mathbf{z}) = \frac{1}{2}(\beta - a, L - a)$ .

gauge fields  $A_\mu(x)$  to smeared gauge fields  $B_\mu(x, t)$ , where  $t$  is the so-called flow time, via the flow equation

$$\partial_t B_\mu = D_\nu F_{\nu\mu}, \quad B_\mu(x, 0) = A_\mu(x). \tag{6}$$

The right-hand side of this differential equation is nothing but the classical equations of motion. Consequently, it will drive the gauge field along the trajectory of steepest descent minimizing the action along the way. On the lattice the simplest form reads

$$a^2 \partial_t V_\mu(x, t) = -g_0^2 \partial_{x,\mu} S_W[V] V_\mu(x, t), \tag{7}$$

where  $V_\mu(x, t)$  is the flowed gauge field with initial condition  $V_\mu(x, 0) = U_\mu(x)$  and  $S_W$  denotes the Wilson plaquette action. The Lie-algebra valued derivative of a general function of the link variables  $f(U_\mu)$  is given by

$$\partial_{x,\mu}^a f(U_\mu(x)) = T^a \frac{d}{ds} f \left( e^{sT^a} U_\mu(x) \right) \Big|_{s=0}. \tag{8}$$

Recently, an  $\mathcal{O}(a^2)$  improved version of the flow equation was developed in Ref. [34]. The so-called Zeuthen flow equation reads

$$a^2 \partial_t V_\mu(x, t) = -g_0^2 \left( 1 + \frac{a^2}{12} \nabla_\mu^* \nabla_\mu \right) \partial_{x,\mu} S_{\text{Sym}}[V] V_\mu(x, t), \tag{9}$$

where  $S_{\text{Sym}}$  is the tree-level improved Symanzik action [46] and the discretized adjoint covariant derivative is given by

$$\begin{aligned} a \nabla_\mu f(x) &= U_\mu(x) f(x + a\hat{\mu}) U_\mu^\dagger(x) - f(x), \\ a \nabla_\mu^* f(x) &= f(x) - U_\mu^\dagger(x - a\hat{\mu}) f(x - a\hat{\mu}) U_\mu(x - a\hat{\mu}). \end{aligned} \tag{10}$$

The unexpected additional factor  $(1 + a^2 \nabla_\mu^* \nabla_\mu / 12)$  can be understood as follows. We know that improvement requires replacing square plaquettes with a linear combination of squares and rectangles. The Symanzik action does this in the four spacetime directions. The added term does it in the flow-time direction. Ref. [34] have proven that this gives a (tree-level)  $\mathcal{O}(a^2)$  improvement of the flow equation. In addition to these two we investigate a flow equation with an overimproved action (precise definitions of these actions are given in Sect. 4.1)

$$a^2 \partial_t V_\mu(x, t) = -g_0^2 (\partial_{x,\mu} S_{\text{OI}}[V]) V_\mu(x, t). \tag{11}$$

We expect this flow equation to allow for stable topological solutions under flow. Notice that the flow equations Eqs. (7), (9), and (11) do not depend on  $g_0^2$  at all since the actions themselves carry such a factor, too. We therefore omit  $g_0^2$  factors when not relevant for the discussion.

The goal is to study the effect of Eqs. (7), (9), and (11) on our constructed clean topological configurations to learn about how their topological properties are changed. This can represent interesting information to better control systematic

errors when performing lattice calculations of topological observables with the help of flow.

### 4 Lattice caloron properties

Mainly we will focus on the measurement of the topological charge  $Q$  and the action  $S$  which in the continuum take the values  $Q = 1$  and  $S = 8\pi^2$ , respectively. Deviations from these numbers occur on a finite lattice due to cutoff and boundary effects. We will try to disentangle those to more deeply understand the effect of flow.

#### 4.1 Actions

Throughout this work we consider Lüscher–Weisz actions of the form [46,47] (omitting  $g_0^2$  factors)

$$S(c_0, c_1) = 2 \left( c_0 \sum_x \text{Re tr} (\mathbb{1} - U_P(x)_{(1,1)}) + c_1 \sum_x \text{Re tr} (\mathbb{1} - U_R(x)_{(2,1)}) \right), \tag{12}$$

where  $U_P(x)_{(1,1)}$  denotes the simple closed plaquette and  $U_R(x)_{(2,1)}$  are  $2 \times 1$  (and  $1 \times 2$ ) rectangles where both loop orientations are taken into account by the  $\text{Re tr}$  operation. A correct normalization requires  $c_0 + 8c_1 = 1$ . The three actions going into the three different flow equations can be summarized as follows:

$$\begin{aligned} S(1, 0) &= S_W && \text{(Wilson),} \\ S(5/3, -1/12) &= S_{\text{Sym}} && \text{(Symanzik),} \\ S(7/3, -1/6) &= S_{\text{OI}} && \text{(Overimproved).} \end{aligned} \tag{13}$$

Figure 1 explores how each action varies as a function of the caloron size  $\rho T$ , on a lattice with  $N_\tau = 8$  and an aspect ratio of 6. We find that all actions start small and are suppressed until about  $\rho = 1.6a$ , which is  $\rho T = 0.2$  for this  $N_\tau$  value. A rapid rise towards the expected value of  $8\pi^2$  is then observed, followed eventually by a rise above  $8\pi^2$ . These two features – the rapid rise from zero towards  $8\pi^2$ , and the eventual rise above this value – arise from different artifacts. The former is a lattice spacing artifact, which we now explore. We overlay each curve with an estimate based on a small- $a$  expansion, taken to first nontrivial subleading order. Specifically, the expansion of the Wilson action in operator dimension takes the form

$$S_W = -\frac{1}{2} \text{tr} \{ F_{\mu\nu} F_{\mu\nu} \} + \frac{a^2}{12} \text{tr} \{ D_\mu F_{\mu\nu} D_\mu F_{\mu\nu} \} + \dots, \tag{14}$$

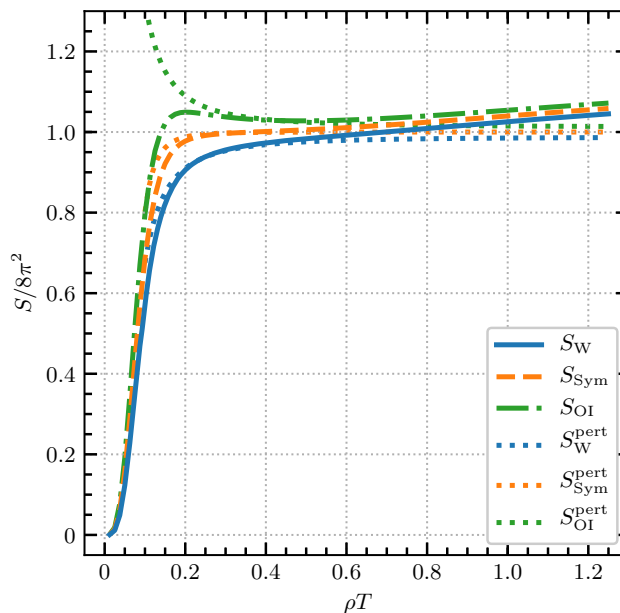


**Fig. 1** Different actions together with the perturbative predictions as a function of the caloron size. The caloron is placed at the center of an  $8 \times 48^3$  lattice. In this plot we used  $t_0 T^2 = 20/64$  for reducing the boundary effects (cf. App. A). Dotted lines indicate a small- $a$  expansion up to the first nontrivial correction

where each index is summed once. This leads to  $a^2$  corrections to the caloron action. Inserting the caloron field from Eqs. (1) and (2), a corresponding finite temperature integration  $\int_0^{1/T} d\tau \int d^3x$  yields

$$S_W = 8\pi^2 \left[ 1 + \mathcal{F}(\rho T) \left( \frac{a}{\rho} \right)^2 + \mathcal{O} \left( \frac{a}{\rho} \right)^4 \right]. \tag{15}$$

We have evaluated  $\mathcal{F}(\rho T)$  numerically and find that it is very well fit by

$$\mathcal{F}(\rho T) = -\frac{1}{5} + b(\rho T)^2 + \mathcal{O}(\rho T)^4, \tag{16}$$

with  $-1/5$  the zero-temperature (instanton) value and  $b = -0.758$ . The first (vacuum) effect is  $\mathcal{O}(a^2/\rho^2)$ ; because of it, the action is significantly smaller for  $\rho < 1.6a$ , and we should consider such objects as “dislocations” rather than true continuum-like calorons. The second term gives rise to an  $\mathcal{O}(a^2 T^2 = 1/N_\tau^2)$  correction, which is present at all caloron sizes, and represents a size-independent mis-estimate of the caloron action due to the lattice spacing. For the overimproved case the  $a^2$  correction is the same but with opposite sign. For the Symanzik case we have not evaluated the full temperature-dependent  $\mathcal{O}(a^4)$  correction, but instead use the  $\mathcal{O}(a^4)$  correction to the instanton action found by Ref. [48]. This is adequate because the correction is small for  $\rho T \sim 1$  where thermal effects are expected.

The overimproved action possesses positive  $a^2$  corrections and therefore develops a maximum. This will be of

importance when flowing with this action as it will stabilize calorons larger than the size where  $S$  is maximum, preventing them from shrinking, “falling through the lattice,” and being lost. As we will see, although promising, this approach does not substantially help in the calculation of the topological susceptibility.

The figure also features a rise in the action above  $8\pi^2$  at large caloron sizes; for the lattice considered in the figure, this effect becomes larger than the  $a^2$  effects above about  $\rho T = 0.7$ . This is a finite-volume effect which is ameliorated by going to a larger aspect ratio. It is also partly an artifact of the way we construct the caloron solution, since we take properly into account the temporal periodicity but not the space periodicity. In order to reduce this effect as much as possible, we “flow the boundaries away.” What this means is that we perform a space-time dependent flow where the core of the configuration (where most of the topological charge is localized) is unaffected while boundary effects are smoothed out. A similar idea was used in Ref. [30] where a discretized version of  $D_\mu F_{\mu\nu}(x)$  was measured on every space-time point and an improved form of cooling was performed on those lattice points that satisfied the bound  $D_\mu F_{\mu\nu}(x) > \epsilon$ . In App. A we explain our own procedure for reducing boundary effects which we utilize throughout this work. From now on, when setting up a topological configuration, we always implicitly apply this procedure. Note that the gradient flow used to reduce the boundary effects should not be confused with the usual gradient flow that we apply for some calculations in the remainder of this work.

### 4.2 Topological charges

The field-strength tensor  $F_{\mu\nu}(x)$  is the main building block for constructing gauge operators like the topological charge. Apart from the popular geometrical clover definition (4-plaquette average), we considered an improved version thereof. To this end, we implement an improved field-strength tensor  $\hat{F}_{\mu\nu}^{\text{imp}}$  free of  $\mathcal{O}(a^2)$  errors by considering weighted averages of  $1 \times 1$  plaquettes and  $2 \times 1$  rectangles [49,50].

We then study the two definitions

$$Q_{\text{clov/imp}} = -\frac{1}{32\pi^2} \epsilon_{\mu\nu\rho\sigma} \sum_x \text{tr} \left( \hat{F}_{\mu\nu}(x) \hat{F}_{\rho\sigma}(x) \right), \quad (17)$$

where in each case

$$\begin{aligned} \hat{F}_{\mu\nu}^{\text{clov}}(x) &= F_{\mu\nu}(x) + \mathcal{O}(a^2), \\ \hat{F}_{\mu\nu}^{\text{imp}}(x) &= F_{\mu\nu}(x) + \mathcal{O}(a^4). \end{aligned} \quad (18)$$

As can be seen from Fig. 2, the improved topological charge operator shows a much better behavior at all investigated values of the radius. Notice that boundary effects are milder

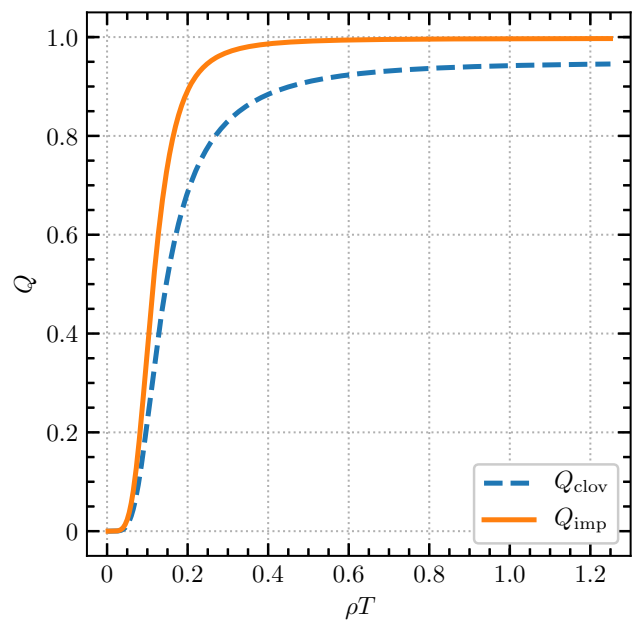


**Fig. 2** Two different discretizations of the topological charge operator as a function of the caloron size on an  $8 \times 32^3$  lattice

for the topological charge than for the action. We see only advantages to using the improved definition.

### 4.3 Critical Radius

One of the relevant aspects we want to address in this paper is the behavior of a discretized caloron configuration under different flow equations. We see in Fig. 2 that, for  $N_\tau = 8$ , a caloron with  $\rho T \gtrsim 0.12$  will have a  $Q$  value larger than  $1/2$ , if the measurement is made before any flow is applied. Of course in practice such a measurement would be impossible, since the  $Q$  of the caloron would be swamped by contributions from nontopological fluctuations. These disappear after a modest amount of gradient flow. But calorons also shrink and tend to disappear as flow is applied, precisely because of the action corrections which we explored in Fig. 1. We illustrate this effect in Fig. 3, which shows how the  $Q$  value changes under flow for a “large” caloron with  $\rho T = 0.5$  on an  $N_\tau = 8$  lattice. We see that, after some amount of time, the measured topological charge abruptly collapses. This occurs because flow causes the caloron to shrink, eventually abruptly shrinking away and disappearing between lattice sites. At least for Wilson and Zeuthen flow, any caloron will eventually disappear in this way. The collapse is slower for Zeuthen flow because of the absence of  $a^2$  lattice-spacing corrections to the action, but the  $a^4$  and finite-volume effects nevertheless eventually lead to collapse. For the overimproved action, the action has a maximum which prevents flow from ever destroying the caloron.

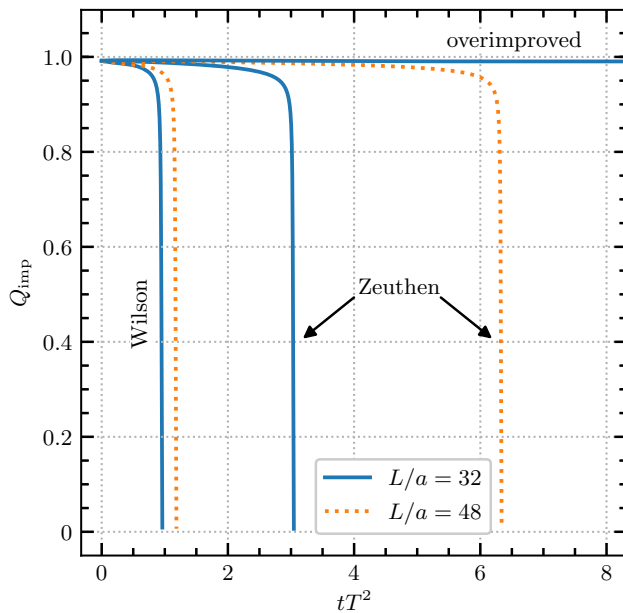


**Fig. 3** Topological charge  $Q_{\text{imp}}$  as a function of flow time for a caloron with  $\rho T = 0.5$ , for three flow definitions and two box sizes ( $N_\tau = 8$  is fixed). Calorons Live much longer under Zeuthen flow, and forever under overimproved flow

It would be very useful to know more precisely, how much flow destroys what size of caloron. To investigate this, we first establish a definition of when we consider a caloron to really exist: when the topological charge  $Q$  exceeds some threshold, which we choose to be  $1/2$ . (We see in Fig. 3 that the exact choice is almost immaterial.) This corresponds well to the typical procedure one will use in determining the topological susceptibility in a simulation: a configuration is generated,  $Q$  is measured, and then its value is thresholded

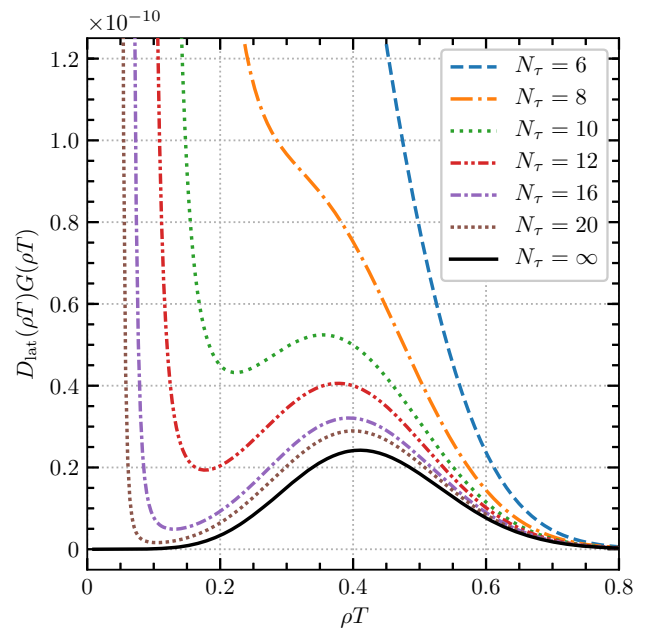


**Fig. 5** Integrand of Eq. (25) at  $T/T_c = 4$  for  $N_\tau = 6, 8, 10, 12, 16, 20$ . The black solid curve represents the continuum case and corresponds to the integrand of Eq. (20)

to an integer. The choice  $1/2$  corresponds to thresholding to the nearest integer. We therefore define the critical radius of a caloron where it becomes topological as

$$Q_{\text{imp}}(\rho_{\text{crit}}) \equiv 0.5. \tag{19}$$

We can then study how flow causes lattice calorons to shrink and disappear by investigating  $\rho_{\text{crit}}$  as a function of flow time, that is, what initial caloron radii  $\rho$  still have  $Q_{\text{imp}} > 0.5$  after some flow depth  $t$ . This is shown in Fig. 4,

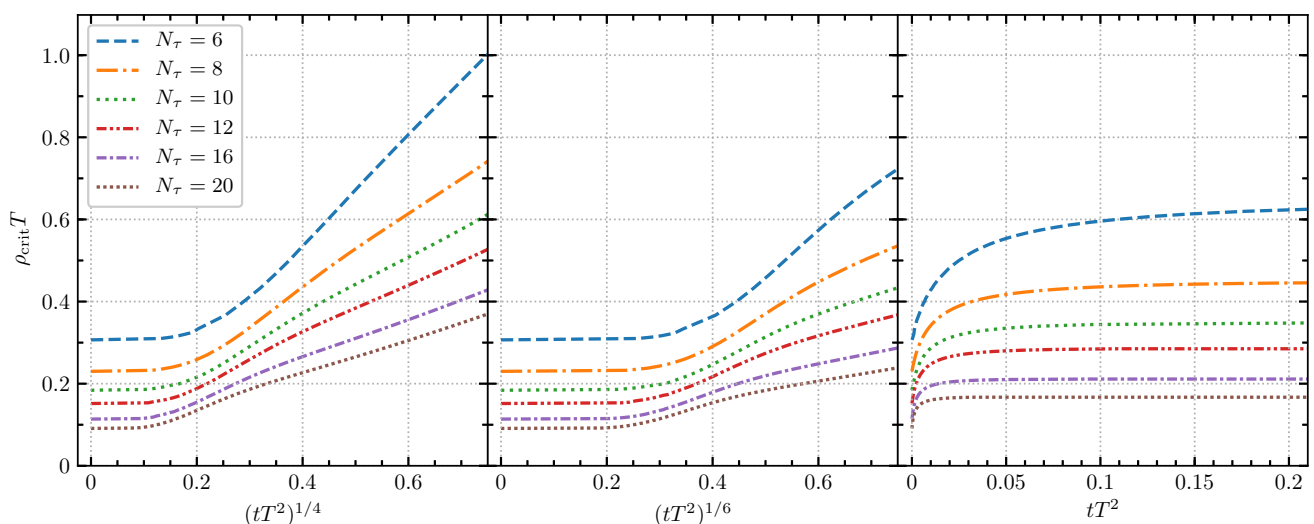


**Fig. 4** Critical caloron radius (separating calorons which survive from those which collapse) as a function of flow depth for three types of flow, and several different temporal lattice extents. Left: Wilson flow. Middle: Zeuthen flow. Right: Overimproved flow

which can be used to look up how much flow is needed to collapse calorons of a given size.

We see in the figure that  $\rho_{\text{crit}}$  grows almost linearly with  $t^{1/4}$ , which is easily explained analytically. An ordinary perturbative fluctuation of momentum  $p$  decays as  $\exp(-p^2 t)$  (this is a leading result coming from Eq. (6)), and so doubling the size requires four times the flow time, or  $t \propto \rho^2$ . However, calorons are nearly extrema of the action, up to  $a^2/\rho^2$  corrections in the Wilson action, so we expect  $t \propto \rho_{\text{crit}}^4$ . Therefore Fig. 4 plots  $\rho_{\text{crit}}$  against  $t^{1/4}$  (Wilson case), which would be a straight line for  $1/N_\tau \ll \rho T \ll 1$ . The figure shows that calorons also collapse under Zeuthen flow, though more slowly (as the energy depends on scale only at  $\mathcal{O}(a^4)$ ), we therefore expect  $t \propto \rho_{\text{crit}}^6$  and, in fact, the curves show a linear trend. Under overimproved flow calorons are preserved above some critical size, which was the original motivation for considering it [48].

### 5 Estimated $a^2$ errors in the topological susceptibility

We want to apply our results to get a semi-analytical understanding of how both flow depth and  $a^2$  errors may influence lattice determinations of the topological susceptibility at high temperatures. Our goal is *not* to calculate the topological susceptibility *per se*, but to see how flow and lattice spacing may influence its determination at finite lattice spacing.

We will do so by approximating the distribution of topological objects using the dilute instanton gas (DIGA) approximation. We incorporate the known one-loop renormalization contributions to the caloron [20], and estimate the topological susceptibility by integrating over all instanton sizes. In the continuum this quantity is given by

$$\chi(T/T_c) \simeq 2 \int_0^{1/\Lambda_{\overline{\text{MS}}}^{N_f=0}} d\rho D(\rho) G(\pi\rho T), \tag{20}$$

with

$$D(\rho) = \frac{d_{\overline{\text{MS}}}}{\rho^5} \left( \frac{8\pi^2}{g^2(\mu = \rho^{-1})} \right)^6 \exp\left( -\frac{8\pi^2}{g^2(\mu = \rho^{-1})} \right), \tag{21}$$

the vacuum density of instantons with size  $\rho$ , and

$$G(\lambda) = \exp\left( -2\lambda^2 - 18A(\lambda) \right), \tag{22}$$

$$A(\lambda) = -\frac{1}{12} \ln\left( 1 + \frac{\lambda^2}{3} \right) + \alpha \left( 1 + \gamma\lambda^{-\frac{3}{2}} \right)^{-8}, \tag{23}$$

the thermal corrections, first computed by Gross, Pisarski, and Yaffe [20]. The parameter values in these expressions are  $\alpha = 0.0128974$ ,  $\gamma = 0.15858$ , and  $d_{\overline{\text{MS}}} = \frac{e^{5/6}}{\pi^2} e^{-4.534122}$ . The running of the coupling  $g^2(\mu)$  can be found in Ref. [51] and  $T_c/\Lambda_{\overline{\text{MS}}}^{N_f=0} = 1.26$  is taken from Ref. [52]. The product of

$D(\rho)$  and of  $G(\pi\rho T)$  in Eq. (20) leads to an integrand with a broad peak near  $\rho T \simeq 0.4$  (solid black curve in Fig. 5), which is then the typical size for the calorons which dominate the topological susceptibility.

In performing a lattice Monte-Carlo study, the practitioner chooses an action for sampling configurations. The choice is logically independent from the choice of action used in gradient flow, but it can be equally impactful. In particular, if the lattice study is based on sampling with the Wilson action, something we assume throughout this section, then the continuum action  $8\pi^2$  in Eq. (21) should be replaced by the lattice Wilson action of a caloron from Eq. (15), leading to an  $a^2$  correction to  $D(\rho)$ :

$$D_{\text{lat}}(\rho, T/T_c, N_\tau) = D(\rho) \exp\left[ -\frac{8\pi^2}{g^2(\mu = \rho^{-1})} \left( \frac{1}{\rho T N_\tau} \right)^2 \mathcal{F}(\rho T) \right]. \tag{24}$$

This rests on an assumption that the coefficient in front of the dimension-6  $a^2$ -suppressed operator ( $DFDF$ ) takes its tree level value. Realistically we expect corrections from, e.g., the renormalization of the  $a^2$  action correction and from higher-order effects in  $G(\pi\rho T)$ , so our results here should be viewed only as estimates, based on the best tools we have available, for how  $a^2$  effects will affect the caloron density on the lattice.

To estimate the topological susceptibility as measured on the lattice, we integrate this modified caloron density over those caloron sizes which are not destroyed by gradient flow – which is precisely all  $\rho > \rho_{\text{crit}}$  as determined in Fig. 4. We therefore write

$$\begin{aligned} \chi_{\text{lat}}(T/T_c, N_\tau, tT^2) &= 2 \int_{\rho_{\text{crit}}(tT^2, N_\tau)}^{1/\Lambda_{\overline{\text{MS}}}^{N_f=0}} d\rho D_{\text{lat}}(\mu = \rho^{-1}, T/T_c) G(\pi\rho T). \end{aligned} \tag{25}$$

We illustrate the integrand for several  $N_\tau$  values in Fig. 5.

Figure 6 shows the resulting estimate of the topological susceptibility which we would obtain by working at a given  $N_\tau$  and applying a given amount of gradient flow. The lattice corrections to the action raise the contributions in the peak of Eq. (20) near  $\rho T \simeq 0.4$ . But lattice artifacts also dramatically increase the number of dislocations with  $\rho \sim a$ , as we see from the integrand in Fig. 5. If these two scales,  $a$  and  $0.4/T$ , are well separated, then gradient flow can erase the dislocations with little impact on the typical calorons. That is, there will be a minimum in the integrand of Fig. 5, and we can use Fig. 4 to choose a flow depth which will erase calorons below this minimum. This leads to a plateau in the susceptibility over a range of flow depths, as seen in Fig. 6. For coarser lattices such as  $N_\tau = 6, 8$ , examining Fig. 5, it

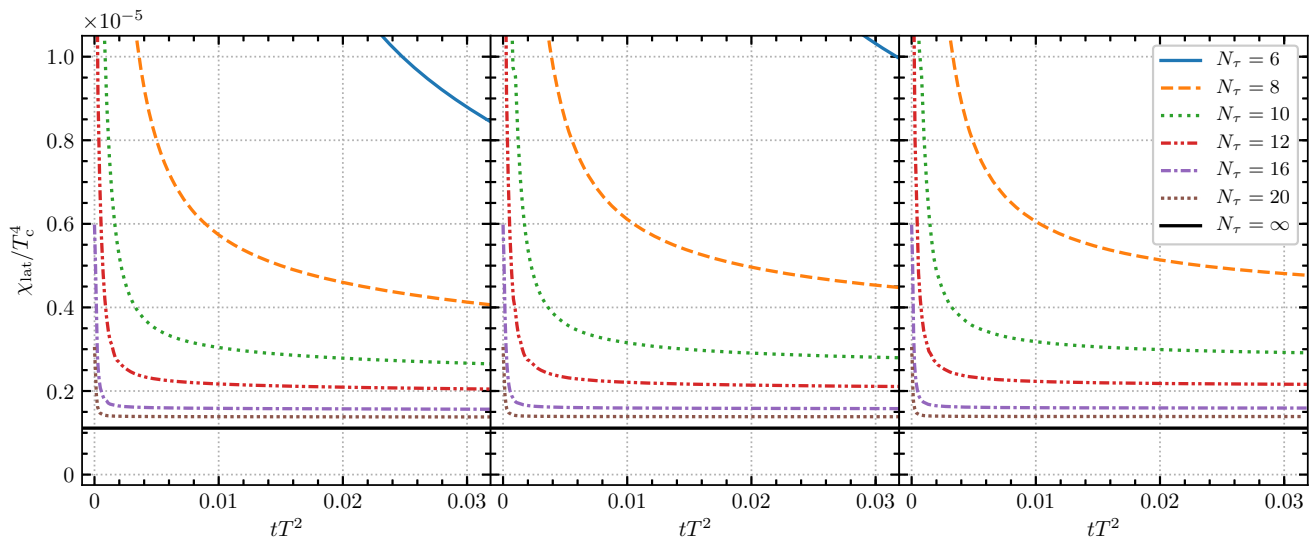


**Fig. 6** Estimated effect of lattice artifacts on the topological susceptibility, at  $T/T_c = 4$  and for  $N_\tau = 6, 8, 10, 12, 16, 20$ , as a function of the flow depth  $tT^2$ . Left: Wilson flow. Middle: Zeuthen flow. Right: Overimproved flow. The solid line denotes the continuum limit

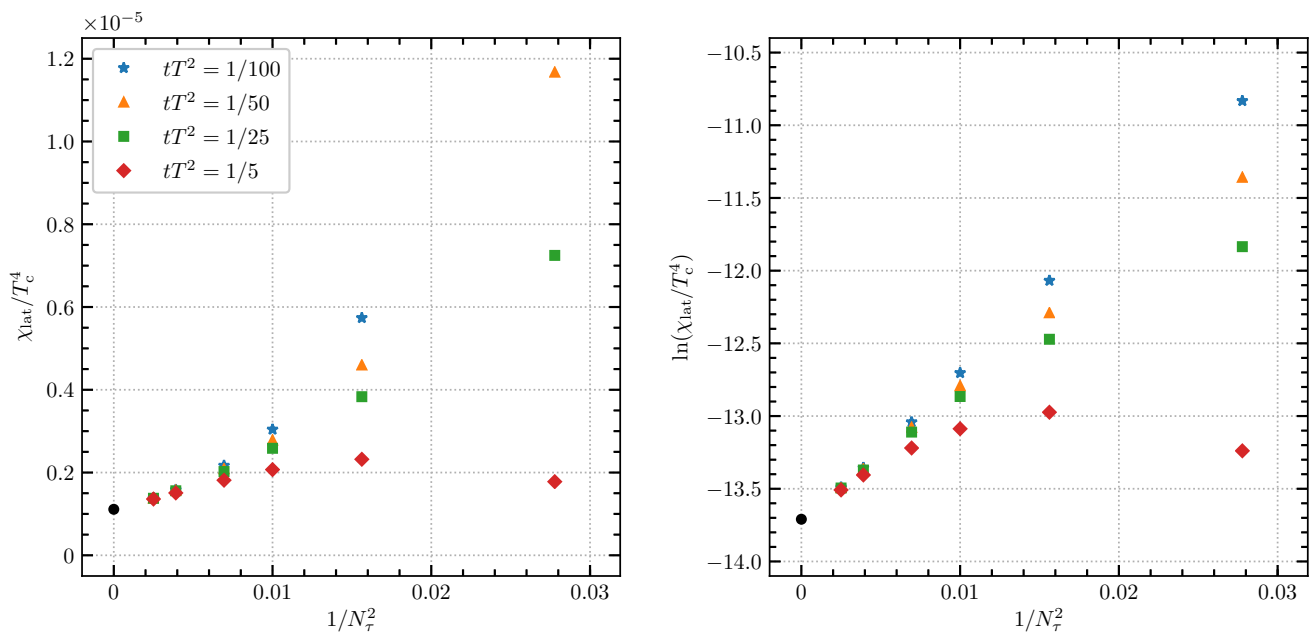


**Fig. 7** Left: Continuum extrapolation Eq. (25) at  $T/T_c = 4$  at fixed (Wilson) flow time. Right: Logarithm of left plot. The black point represents the continuum value

is not clear where to cut to separate calorons from dislocations, and there is no associated plateau in Fig. 6. Therefore  $N_\tau = 6, 8$  will likely not be sufficient to give results which are stable against the amount of flow, but larger  $N_\tau$  will, especially if we use Zeuthen flow. Overimproved flow is good for completely “cleaning” a configuration of perturbative fluctuations, but in terms of eliminating small instantons, it is effectively equivalent to using a specific fixed depth of Wilson flow. Therefore it is not preferred if we want flexibility

in choosing the size of caloron/dislocation which we eliminate.

Finally, we consider the extrapolation to zero lattice spacing in Fig. 7. The lattice spacing corrections are very large even for  $N_\tau = 10$ , and a simple extrapolation in  $\chi$  can easily lead to a negative result. But that is because the  $a^2$  errors are best viewed as a correction to the *logarithm* of  $\chi$ , as we see in Eq. (24). If we extrapolate in terms of  $\ln(\chi)$ , the procedure works much better.



### 6 Conclusions

We have constructed calorons on the lattice. We find that they possess most of the action and topological charge if  $\rho T \gtrsim 1/N_\tau$ , and nearly all of the charge and action if  $\rho T \gtrsim 2/N_\tau$ . Wilson flow destroys small calorons, with progressively more flow destroying larger calorons, as expected. Our work expresses this in a quantitative fashion, in Fig. 4.

Also, if a lattice study were to flow each topologically nontrivial configuration until it loses topological character ( $Q_{\text{imp}} < 0.5$ ), and keep track of the distribution of flow depths needed, then a plot as the one in Fig. 3 could be used to turn this result into a size distribution of the topological objects observed on the lattice.

Using our results to estimate the  $a^2$  errors which arise when computing the topological susceptibility  $\chi(T)$  on the lattice, we find that  $N_\tau = 6$  is insufficient to be in the scaling regime (probably  $N_\tau = 8$  as well), and lattice spacing errors are expected to lead to a severe overestimate of  $\chi(T)$  at finite  $a$ , which may lead to negative values if we extrapolate  $\chi(T)$  against  $a^2$ . It is more natural to extrapolate  $\ln(\chi(T))$  against  $a^2$ , because this corresponds better to the way in which  $a^2$  errors enter in the susceptibility.

Note that the inclusion of light quarks in Eq. (22) would change the factor  $-2\lambda^2$  to  $-(2 + N_f/3)\lambda^2$ , which makes the dominant size of calorons smaller. Therefore, since  $\rho T N_\tau$  becomes smaller, the corrections in Eq. (24) become larger (since  $\mathcal{F}$  is negative), and the value of  $N_\tau$  needed to reach scaling will be still larger.

**Acknowledgements** The authors acknowledge support by the Deutsche Forschungsgemeinschaft (DFG) through the grant CRC-TR 211 ‘‘Strong-interaction matter under extreme conditions’’. We also thank the GSI Helmholtzzentrum and the TU Darmstadt and its Institut

für Kernphysik for supporting this research. This work was performed using the framework of the publicly available openQCD-1.6 package [47]. The authors want to especially thank Marc Wagner and Margarita García-Pérez for interesting discussions at early stages of this work.

**Data Availability Statement** This manuscript has no associated data or the data will not be deposited. [Authors’ comment: This is a theoretical work. No experimental data was used.]

**Open Access** This article is distributed under the terms of the Creative Commons Attribution 4.0 International License (<http://creativecommons.org/licenses/by/4.0/>), which permits unrestricted use, distribution, and reproduction in any medium, provided you give appropriate credit to the original author(s) and the source, provide a link to the Creative Commons license, and indicate if changes were made. Funded by SCOAP<sup>3</sup>.

### A reducing boundary effects

In writing down caloron field configurations, we cannot avoid the discontinuity at the spatial boundaries of our box. We will try to minimize the damage by smearing out the boundary discontinuities with gradient flow. Consider the caloron placed at the center of the lattice and denote the lattice spatial extent as  $L$ . We then flow the links using a flow time that depends on the relative distance

$$d = \sqrt{(x - z)^2} \tag{26}$$

of the base point of the link  $U_\mu(x)$  and the center of the instanton. The flow time depth gets modified as

$$t(d) = \begin{cases} 0, & d < \frac{L}{4} \\ \frac{t_0}{2} \left( 1 + \sin \left[ \frac{4\pi}{L} \left( d - \frac{3}{8}L \right) \right] \right), & \frac{L}{4} \leq d \leq \frac{L}{2} \\ t_0, & d > \frac{L}{2} \end{cases} \tag{27}$$

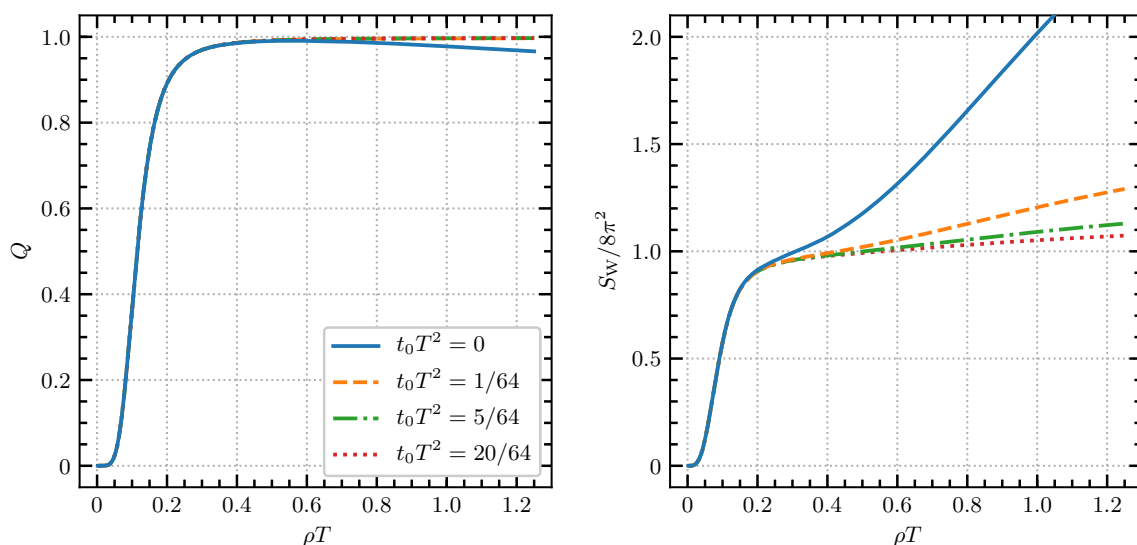


**Fig. 8** Caloron topological charge (left) and Wilson action (right) for different values of  $t_0 T^2$  as defined in Eq. (27) on an  $8 \times 48^3$  lattice

where  $t_0$  is the “normal” flow time. This is nothing but a smooth interpolation between zero flow (close to the center of the caloron) and full flow (close to the boundary). With this procedure we reduce boundary effects while the core of the caloron remains unaffected. In Fig. 8 we show both the topological charge and the Wilson action of the caloron for different values of  $t_0$ . We observe that the Wilson action suffers significantly more from boundary effects than the topological charge. Applying this modified version of Wilson flow indeed reduces boundary effects. We find that a flow time of  $t_0 T^2 = 5/N_\tau^2$  is sufficient to satisfactorily reduce most of the boundary effects.

## References

1. T. Schäfer, E.V. Shuryak, Instantons in QCD. *Rev. Mod. Phys.* **70**, 323–426 (1998). [arXiv:hep-ph/9610451](#)
2. R. Peccei, H.R. Quinn, Constraints imposed by CP conservation in the presence of instantons. *Phys. Rev. D* **16**, 1791–1797 (1977)
3. S. Weinberg, A new light boson? *Phys. Rev. Lett.* **40**, 223–226 (1978)
4. F. Wilczek, Problem of strong p and t invariance in the presence of instantons. *Phys. Rev. Lett.* **40**, 279–282 (1978)
5. J. Preskill, M.B. Wise, F. Wilczek, Cosmology of the invisible axion. *Phys. Lett. B* **120**, 127–132 (1983)
6. L.F. Abbott, P. Sikivie, A cosmological bound on the invisible axion. *Phys. Lett. B* **120**, 133–136 (1983)
7. M. Dine, W. Fischler, The not so harmless axion. *Phys. Lett. B* **120**, 137–141 (1983)
8. G. Grilli di Cortona, E. Hardy, J.P. Vega, G. Villadoro, The QCD axion, precisely. *JHEP* **01**, 034 (2016). [arXiv:1511.02867](#)
9. V.B. Klaer, G.D. Moore, The dark-matter axion mass. *JCAP* **1711**, 049 (2017). [arXiv:1708.07521](#)
10. G.D. Moore, Axion dark matter and the lattice. *EPJ Web Conf.* **175**, 01009 (2018). [arXiv:1709.09466](#)
11. E. Berkowitz, M.I. Buchoff, E. Rinaldi, Lattice QCD input for axion cosmology. *Phys. Rev. D* **92**, 034507 (2015). [arXiv:1505.07455](#)
12. S. Borsanyi, M. Dierigl, Z. Fodor, S.D. Katz, S.W. Mages, D. Nogradi et al., Axion cosmology, lattice QCD and the dilute instanton gas. *Phys. Lett. B* **752**, 175–181 (2016). [arXiv:1508.06917](#)
13. P. Petreczky, H.-P. Schadler, S. Sharma, The topological susceptibility in finite temperature QCD and axion cosmology. *Phys. Lett. B* **762**, 498–505 (2016). [arXiv:1606.03145](#)
14. Y. Taniguchi, K. Kanaya, H. Suzuki, T. Umeda, Topological susceptibility in finite temperature (2+1)-flavor QCD using gradient flow. *Phys. Rev. D* **95**, 054502 (2017). [arXiv:1611.02411](#)
15. F. Burger, E.-M. Ilgenfritz, M.P. Lombardo, M. Müller-Preussker, A. Trunin, Topology (and axion’s properties) from lattice QCD with a dynamical charm. *Nucl. Phys. A* **967**, 880–883 (2017). [arXiv:1705.01847](#)
16. J. Frison, R. Kitano, H. Matusufuru, S. Mori, N. Yamada, Topological susceptibility at high temperature on the lattice. *JHEP* **09**, 021 (2016). [arXiv:1606.07175](#)
17. S. Borsanyi et al., Calculation of the axion mass based on high-temperature lattice quantum chromodynamics. *Nature* **539**, 69–71 (2016). [arXiv:1606.07494](#)
18. P.T. Jahn, G.D. Moore, D. Robaina,  $\chi_{\text{top}}(T \gg T_c)$  in pure-gluon QCD through reweighting. *Phys. Rev. D* **98**, 054512 (2018). [arXiv:1806.01162](#)
19. I. G. Irastorza and J. Redondo, New experimental approaches in the search for axion-like particles. [arXiv:1801.08127](#)
20. D.J. Gross, R.D. Pisarski, L.G. Yaffe, QCD and instantons at finite temperature. *Rev. Mod. Phys.* **53**, 43 (1981)
21. A.D. Linde, Infrared problem in thermodynamics of the Yang-Mills gas. *Phys. Lett.* **96B**, 289–292 (1980)
22. M. Lüscher, Topology of lattice gauge fields. *Commun. Math. Phys.* **85**, 39 (1982)
23. P.H. Ginsparg, K.G. Wilson, A remnant of chiral symmetry on the lattice. *Phys. Rev. D* **25**, 2649 (1982)
24. H. Neuberger, Exactly massless quarks on the lattice. *Phys. Lett. B* **417**, 141–144 (1998). [arXiv:hep-lat/9707022](#)
25. M. Luscher, Exact chiral symmetry on the lattice and the Ginsparg-Wilson relation. *Phys. Lett. B* **428**, 342–345 (1998). [arXiv:hep-lat/9802011](#)
26. R. Narayanan, H. Neuberger, Infinite N phase transitions in continuum Wilson loop operators. *JHEP* **03**, 064 (2006). [arXiv:hep-th/0601210](#)
27. M. Lüscher, Trivializing maps, the Wilson flow and the HMC algorithm. *Commun. Math. Phys.* **293**, 899–919 (2010). [arXiv:0907.5491](#)
28. B. Berg, Dislocations and topological background in the lattice O(3)  $\sigma$  model. *Phys. Lett. B* **104**, 475–480 (1981)
29. P. de Forcrand, M. Garcia Perez, I.-O. Stamatescu, Topology of the SU(2) vacuum: a lattice study using improved cooling. *Nucl. Phys. B* **499**, 409–449 (1997). [arXiv:hep-lat/9701012](#)
30. M. Garcia Perez, O. Philipsen, I.-O. Stamatescu, Cooling, physical scales and topology. *Nucl. Phys. B* **551**, 293–313 (1999). [arXiv:hep-lat/9812006](#)
31. M. Garcia Perez, A. Gonzalez-Arroyo, A. Montero, P. van Baal, Calorons on the lattice: a new perspective. *JHEP* **06**, 001 (1999). [arXiv:hep-lat/9903022](#)
32. M. Teper, Instantons in the quantized SU(2) vacuum: a lattice Monte Carlo investigation. *Phys. Lett. B* **162**, 357–362 (1985)
33. B.J. Harrington, H.K. Shepard, Periodic Euclidean solutions and the finite temperature Yang-Mills gas. *Phys. Rev. D* **17**, 2122 (1978)
34. A. Ramos, S. Sint, Symanzik improvement of the gradient flow in lattice gauge theories. *Eur. Phys. J. C* **76**, 15 (2016). [arXiv:1508.05552](#)
35. D.J.R. Pugh, M. Teper, Topological dislocations in the continuum limit of SU(2) lattice gauge theory. *Phys. Lett. B* **224**, 159–165 (1989)
36. F. Bruckmann, D. Nogradi, P. van Baal, Higher charge calorons with non-trivial holonomy. *Nucl. Phys. B* **698**, 233–254 (2004). [arXiv:hep-th/0404210](#)
37. F. Bruckmann, E.M. Ilgenfritz, B.V. Martemyanov, M. Müller-Preussker, D. Nogradi, D. Peschka et al., Calorons with non-trivial holonomy on and off the lattice. *Nucl. Phys. Proc. Suppl.* **140**, 635–646 (2005). [arXiv:hep-lat/0408036](#)
38. P. de Forcrand, M. Garcia Perez, I.-O. Stamatescu, Improved cooling algorithm for gauge theories. *Nucl. Phys. Proc. Suppl.* **47**, 777–780 (1996). [arXiv:hep-lat/9509064](#)
39. P. de Forcrand, S. Kim, Topological susceptibility and instanton size distribution from over improved cooling. *Nucl. Phys. Proc. Suppl.* **47**, 278–281 (1996). [arXiv:hep-lat/9509081](#)
40. G. ’t Hooft, Symmetry breaking through Bell–Jackiw anomalies. *Phys. Rev. Lett.* **37**, 8–11 (1976)
41. R. Jackiw, C. Nohl, C. Rebbi, Conformal properties of pseudoparticle configurations. *Phys. Rev. D* **15**, 1642 (1977)
42. M. Lüscher, Properties and uses of the Wilson flow in lattice QCD. *JHEP* **08**, 071 (2010). [arXiv:1006.4518](#)
43. M. Lüscher, Topology, the Wilson flow and the HMC algorithm. *PoS LATTICE2010*, 015 (2010). [arXiv:1009.5877](#)
44. M. Lüscher, P. Weisz, Perturbative analysis of the gradient flow in non-abelian gauge theories. *JHEP* **02**, 051 (2011). [arXiv:1101.0963](#)
45. M. Lüscher, Chiral symmetry and the Yang-Mills gradient flow. *JHEP* **04**, 123 (2013). [arXiv:1302.5246](#)

46. M. Lüscher, P. Weisz, On-shell improved lattice gauge theories. *Commun. Math. Phys.* **97**, 59 (1985)
47. <http://luscher.web.cern.ch/luscher/openQCD/index.html>
48. M Garcia Perez, A. Gonzalez-Arroyo, J. R. Snippe, P. van Baal, Instantons from over—improved cooling. *Nucl. Phys. B* **413**, 535–552 (1994). [arXiv:hep-lat/9309009](https://arxiv.org/abs/hep-lat/9309009)
49. G.D. Moore, Improved Hamiltonian for Minkowski Yang-Mills theory. *Nucl. Phys. B* **480**, 689–728 (1996). [arXiv:hep-lat/9605001](https://arxiv.org/abs/hep-lat/9605001)
50. S.O. Bilson-Thompson, D.B. Leinweber, A.G. Williams, Highly improved lattice field strength tensor. *Ann. Phys.* **304**, 1–21 (2003). [arXiv:hep-lat/0203008](https://arxiv.org/abs/hep-lat/0203008)
51. K.G. Chetyrkin, B.A. Kniehl, M. Steinhauser, Decoupling relations to  $O(\alpha_s^3)$  and their connection to low-energy theorems. *Nucl. Phys. B* **510**, 61–87 (1998). [arXiv:hep-ph/9708255](https://arxiv.org/abs/hep-ph/9708255)
52. S. Borsanyi, G. Endrodi, Z. Fodor, S.D. Katz, K.K. Szabo, Precision SU(3) lattice thermodynamics for a large temperature range. *JHEP* **07**, 056 (2012). [arXiv:1204.6184](https://arxiv.org/abs/1204.6184)